

# Nonrigid Multimodal Registration Based on Fuzzy Inference System for Retinal Image Registration

## Abstract

**Background:** Retinal imaging employs various modalities, each providing distinct perspectives on ocular structures. However, the integration of information from these modalities, which often have differing resolutions, requires effective image registration techniques. Existing retinal image registration methods typically rely on rigid or affine transformations, which may not adequately address the complexities of multimodal retinal images. **Method:** This study introduces a nonrigid fuzzy image registration approach designed to align optical coherence tomography (OCT) images with fundus images. The method employs a fuzzy inference system (FIS) that uses vessel locations as key features for registration. The FIS applies specific rules to map points from the source image to the reference image, facilitating accurate alignment. **Results:** The proposed method achieved a mean absolute registration error of  $44.57 \pm 39.38 \mu\text{m}$  in the superior–inferior orientation and  $11.46 \pm 10.06 \mu\text{m}$  in the nasal-temporal orientation. These results underscore the method's precision in aligning multimodal retinal images. **Conclusion:** The nonrigid fuzzy image registration approach demonstrates robust and versatile performance in integrating multimodal retinal imaging data. Despite its straightforward implementation, the method effectively addresses the challenges of multimodal retinal image registration, providing a reliable tool for advanced ocular imaging analysis.

**Keywords:** Fundus, fuzzy, multimodal registration, nonrigid image registration, optical coherence tomography

Submitted: 14-Jun-2024

Revised: 14-Oct-2024

Accepted: 22-Oct-2024

Published: 01-May-2025

## Introduction

Fundus imaging and optical coherence tomography (OCT) are ubiquitous modalities in retinal imaging, frequently employed in clinical practice for their ability to capture detailed images of the retina.<sup>[1,2]</sup> Often, these two modalities are utilized simultaneously during retinal examinations, providing complementary information about retinal structures and pathology.<sup>[3,4]</sup> The integration of data from both fundus images and OCT scans holds immense potential for advancing diagnostic capabilities and guiding treatment decisions in ophthalmology.<sup>[4]</sup> By leveraging the rich information conveyed by these modalities, clinicians can conduct more comprehensive analyses and gain deeper insights into retinal health and disease progression. Recently, the application of en face image registration for identifying ocular imaging biomarkers has been reported.<sup>[5]</sup>

This is an open access journal, and articles are distributed under the terms of the Creative Commons Attribution-NonCommercial-ShareAlike 4.0 License, which allows others to remix, tweak, and build upon the work non-commercially, as long as appropriate credit is given and the new creations are licensed under the identical terms.

For reprints contact: WKHLRPMedknow\_reprints@wolterskluwer.com

Furthermore, en face/fundus alignment is often a critical preliminary step in various OCT processing methods. For example, in<sup>[6,7]</sup> aligning OCT B-scans of the left and right eyes is necessary. However, direct alignment of OCT B-scans is challenging because the fovea and optic disc positions cannot always be reliably detected from the B-scans alone. This requires the use of fundus images to identify the fovea and optic disc locations. Once the left and right fundus images are aligned, the corresponding en face images can be registered, ensuring that the left and right en face images are correctly aligned. Finally, the geometric transformation obtained between the en face and fundus images should be applied to the OCT B-scans. However, multimodal image registration including en face/fundus registration poses several challenges stemming from inherent differences in image characteristics, including resolution, contrast, and geometric distortions. Moreover, variations in imaging conditions and technical artifacts further complicate the registration process.

**How to cite this article:** Hosseini MS, Rabbani H. Nonrigid multimodal registration based on fuzzy inference system for retinal image registration. *J Med Signals Sens* 2025;15:13.

**Monire Sheikh Hosseini, Hossein Rabbani**

*Medical Image and Signal Processing Research Center, School of Advanced Technology in Medicine, Isfahan University of Medical Science, Isfahan, Iran*

## Address for correspondence:

*Dr. Monire Sheikh Hosseini, Medical Image and Signal Processing Research Center, School of Advanced Technology in Medicine, Isfahan University of Medical Science, Isfahan, Iran.*

*E-mail: sheikhhosseini.m@gmail.com; m.sheikhhosseini@amt.mui.ac.ir*

## Access this article online

Website: [www.jmssjournal.net](http://www.jmssjournal.net)

DOI: 10.4103/jmss.jmss\_42\_24

## Quick Response Code:



To register en face and fundus images, proper features should be extracted from both modalities. In many reported works, vessel features<sup>[8,9]</sup> or features extracted from vessels, such as vessel ridges<sup>[10]</sup> are utilized for registration, as vessels are the most common information shared between the two modalities. Furthermore, given that, the OCT B-scans are obtained from the macula; the estimated macula position in the fundus image is used to determine the corresponding OCT scanning area. It means that the OCT scanning area may be unknown and should be determined through the registration process. For instance, in<sup>[8]</sup> a square with 25 different central points of the fundus image is explored around the approximate point corresponding to the center of the OCT image. In<sup>[7]</sup> a method is used where the correlation between vessels in two image modalities is computed by rotating the en face image at different angles and selecting the angle with the highest correlation to align the fundus and en face images. In<sup>[6]</sup> and<sup>[11]</sup> a similarity function is utilized to determine the optimal shift, rotation, and scaling between the fundus and en face images.

It is worth noting that, in most retinal image registration algorithms, whether monomodal or multimodal, the registration step typically employs classical methods. Even, recent approaches that incorporate deep learning still rely on techniques such as rigid,<sup>[5]</sup> affine,<sup>[9]</sup> random sample consensus (RANSAC),<sup>[12]</sup> weighted direct linear transforms,<sup>[13]</sup> or other classic methods. Therefore, classic successful algorithms are chosen for comparison. The assumption of rigid transformation between the fundus and OCT modalities may not hold true due to the differing methods of image acquisition. Therefore, we believe that nonrigid registration may be a more reasonable choice. In this context, nonrigid image registration techniques prove valuable for aligning images exhibiting varying geometric transformations.

From another point of view, the fuzzy concept demonstrates powerful performance in various image processing fields such as segmentation,<sup>[14]</sup> classification,<sup>[15]</sup> and registration.<sup>[16]</sup> Recently, fuzzy inference systems (FISs) have emerged as powerful tools for capturing intricate relationships between input and output variables in monomodal image registration.<sup>[17]</sup> This article aims to demonstrate the effectiveness of FIS in the context of multimodal retinal image registration. Therefore, the proposed method is conceptually new because, to the best of our knowledge, retinal image registration based on fuzzy systems has not been introduced in the literature, particularly the multimodal retinal registration. Moreover, in applications where the ultimate goal of en face/fundus registration is the alignment of B-scans from the left and right eyes, our approach offers a more precise solution. Specifically, rather than applying a uniform rigid transformation to all B-scans, we propose using a nonrigid transformation tailored to each B-scan. This approach allows for a unique transformation to be applied to each A-scan within the B-scans, which

is more accurate and reasonable than applying the same transformation across all A-scans or B-scans. It is worth noting that the proposed method is not sensitive to image scales. In addition, any potential weaknesses in determining OCT scanning area can be compensated by the fuzzy rules. This is because the fuzzy theory is designed to model uncertainties, allowing the fuzziness of the OCT scanning window to be indirectly addressed through the fuzzy system.

The remainder of the article is organized as follows. Section 2 provides a detailed description of the proposed algorithm for en face/fundus registration. Section 3 covers the data description and implementation details. Experimental results are presented in Section 4 and conclusions are drawn in Section 6.

## Methods

The proposed method's block diagram is depicted in Figure 1. Initially, the OCT B-scans are projected to generate an en face image, which serves as the basis for registration with the fundus image. The registration process begins with the extraction of retinal vessels from both the fundus and en face images. Next, a window surrounding the approximate central point of the fundus image is selected, where the highest correlation with the en face vessel map is found. Corresponding points on the vessels in both images are then identified, forming input–output pairs for designing the FIS, and the mapped vessels are subsequently calculated. Each step is described in detail below. In the figure, the green and magenta points correspond to the fundus and en face images, respectively, while the yellow points represent the vessels from the en face image mapped onto the fundus image.

### Projecting optical coherence tomography B-scans

To construct a two-dimensional (2D) en face image, the 3D OCT volumes can be projected along the depth axis. Various metrics, such as the mean, maximum, minimum, or standard deviation of pixel values along the depth axis, can be used for this projection.<sup>[7]</sup> In this study, the standard deviation of A-scans from OCT slices is used to create the en face image, as illustrated in Figure 2.

### Vessel extraction

The U-Net architecture<sup>[18]</sup> has emerged as a widely adopted method in medical image segmentation, including retinal vessel segmentation.<sup>[19]</sup> Because of effectiveness even with limited training samples,<sup>[19]</sup> we employed the U-Net method for vessel extraction for both the en face and the fundus images. The U-Net model follows the conventional U-Net architecture, as shown in Figure 3. The encoder part of the network consists of five contracting blocks, with each block doubling the number of feature maps. The feature map sizes are reduced by a factor of two after each max-pooling operation. Starting with 64 feature maps of size  $256 \times 256$

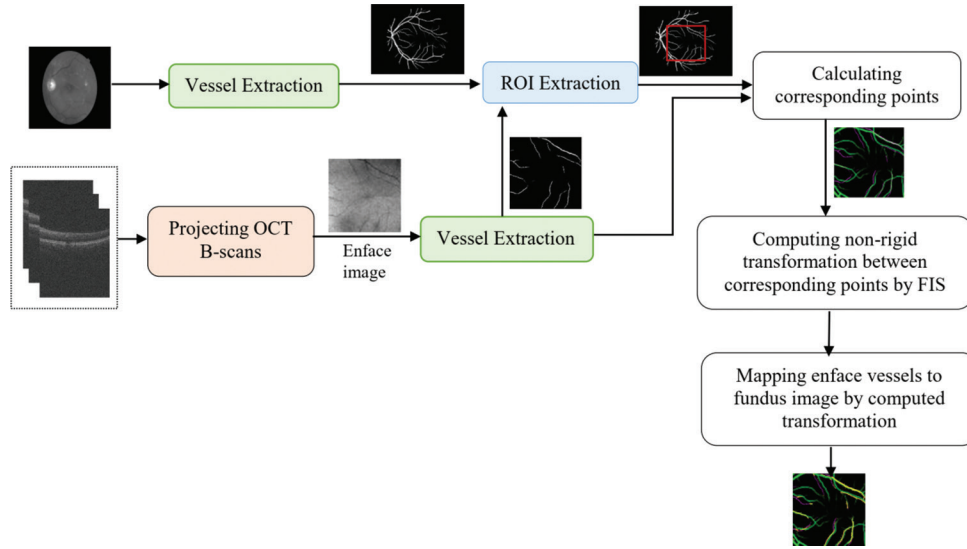


**Figure 1: Block diagram of the proposed method for en face/fundus registration. The vessels in fundus and en face images are illustrated in green and magenta, respectively. The registered vessels are shown in yellow. OCT: Optical coherence tomography, ROI: Region of interest, FIS: Fuzzy inference system**

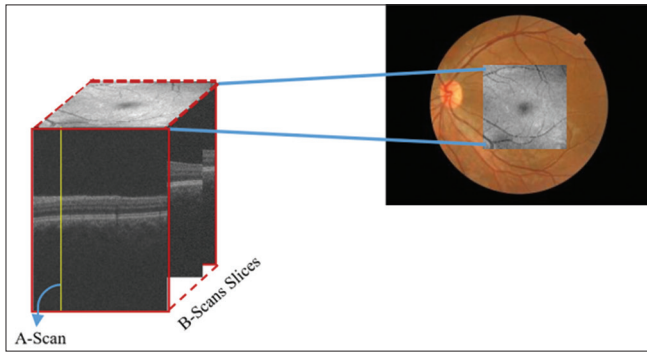


**Figure 2: The color fundus image (right) and the corresponding en face image (grayscale, smaller image on the right). The en face image is created by projecting the B-scans along the depth axis**

in the first block, the number of feature maps increases to 128 ( $128 \times 128$ ), 256 ( $64 \times 64$ ), 512 ( $32 \times 32$ ), and finally 1024 ( $16 \times 16$ ) in the deepest part of the network. The decoder mirrors this structure with upsampling, where feature map sizes increase back to  $256 \times 256$ , and the number of channels decreases symmetrically to 512, 256, 128, and 64. The training procedure utilizes rectified linear units (ReLUs) and an Adam optimizer. Data augmentation techniques applied to the training data include rotation, flipping, scaling, and cropping.

### Region of interest extraction

The vessel maps obtained from the previous step are  $256 \times 256$  pixels. To select the region of interest in the fundus image, a  $20 \times 20$  pixel square around the center of the fundus vessel map is chosen as the search area for the window's center. Windows with edge lengths ranging from 90 to 140 pixels are examined for each possible center. These windows are then resized to  $256 \times 256$  pixels, and their correlation with the en face vessel map is computed. The best match is selected as the final OCT scanning

area [Figure 4]. It is important to note that the correlation between these two images may not be very high, as achieving a higher correlation would typically require at least a rotation. However, since the proposed registration method can effectively find the mapping with a limited number of corresponding points, this issue is not a major concern.

### Registration method

The block diagram of the registration phase is illustrated in Figure 5. Points located on the en face image are first processed using the Density-Based Spatial Clustering of Applications with Noise algorithm<sup>[20]</sup> to determine the optimal number of clusters for the fuzzy C-Means (FCM) clustering algorithm.<sup>[21]</sup> Subsequently, the points are clustered using FCM, and the membership degree of each point to each cluster is calculated. Finally, the clustered points and their corresponding points on the fundus image are used to train a Takagi-Sugeno-Kang (TSK) model,<sup>[22,23]</sup> which is then employed to calculate the mapped points. The core of the proposed method is a FIS, which combines the FCM clustering algorithm with the TSK model, as described in detail below.

### Fuzzy inference system

Consider that the proposed method incorporates  $R$  rules in the FIS part. Each rule can be represented as follows:

$$\begin{aligned} & \text{if } x_{1m} \text{ is } F_1^r \text{ and } x_{2m} \text{ is } F_2^r \text{ then} \\ & \hat{y}_{im}^r = p_{0i}^r + p_{1i}^r x_{1m} + p_{2i}^r x_{2m} \end{aligned} \quad (1)$$

where  $F_1^r$  and  $F_2^r$  are fuzzy sets of the  $r^{\text{th}}$  rule.  $x_{1m}$  and  $x_{2m}$  are coordinates of the  $m^{\text{th}}$  point located at the vessel of en face image, while  $\hat{y}_{im}^r$  is estimated coordinate of corresponding point located at the vessel of fundus image in  $i^{\text{th}}$  dimension ( $i = 1, 2$ ). To achieve an optimal structure

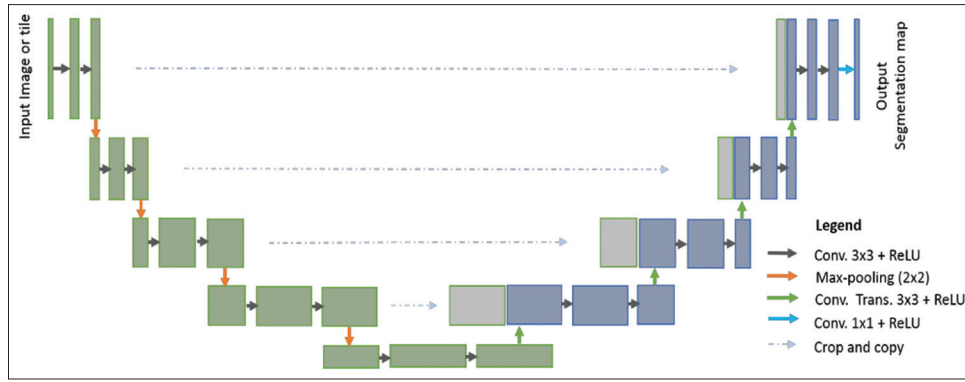
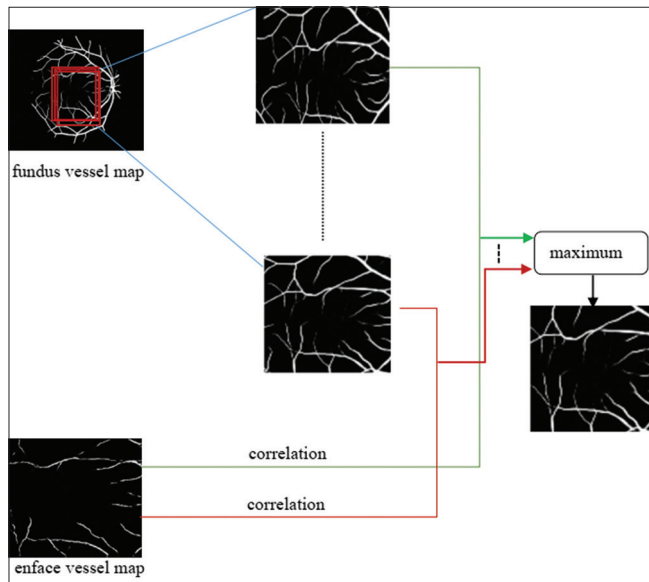

 Figure 3: Conventional U-Net architecture<sup>[19]</sup>


Figure 4: Region of interest extraction procedure

and identify parameters, both premise and consequent structures must be designed. Through this process, the position of each arbitrary point can be calculated using the designed rules.

Let  $(x_m, y_m)$ ,  $m = 1, \dots, M$  be input-output pairs of a FIS that we aim to find their mathematical relation. In our problem,  $x_m = (x_{1m}, x_{2m})$  and  $y_m = (y_{1m}, y_{2m})$  represent the coordinates of points located on the source image (en face) and the reference (fundus) image, respectively. The optimal parameters and structure of the aforementioned system are obtained through the design of antecedent and consequent structures.

#### Antecedent part of fuzzy rules

Various methods exist for configuring the premise part of the FIS. One commonly employed and well-established approach is the FCM clustering algorithm.<sup>[21]</sup> The FCM algorithm calculates cluster centers,  $v$ , and membership degree of each sample to each cluster,  $u$ , by solving the optimization problem as depicted in equation (2).

$$\min J(u, v) = \sum_{k=1}^M \sum_{i=1}^c (u_{ik})^2 \cdot (d_{ik})^2 \quad (2)$$

where  $d_{ik} = \|x_k - v_i\|^2$  is the distance of sample  $x_k \in \mathbb{R}^2$  from the cluster center  $v_i$ . The algorithm initializes with a predefined cluster number, and initial guesses for cluster centers,  $V = (v_1, \dots, v_c)$ , and continues by updating cluster centers,  $V$ , and membership degree,  $u = (u_{1m}, \dots, u_{cm})$ , through (3)–(4) until convergence.

$$v_i = \frac{\sum_{k=1}^M u_{ik} x_k}{\sum_{k=1}^M u_{ik}} \quad (3)$$

$$u_{ik} = \left[ \sum_{j=1}^c \left( \frac{d_{jk}}{d_{ik}} \right)^2 \right]^{-1} \quad \text{for } \forall i, k \quad (4)$$

#### Consequent part of fuzzy rules

Assuming a t-norm product, Larsen fuzzy inference (product), and weighted output, the TSK model's overall output, based on the sample rule in (1), is calculated as follows:<sup>[24]</sup>

$$\omega^r(x_m) = \bigwedge_{i \in \{1, \dots, n\}} F_i^r(x_{im}) = \prod_{i \in \{1, \dots, n\}} F_i^r(x_{im}) \quad (5)$$

$$v^r(x_m) = \frac{\omega^r(x_m)}{\sum_{r=1}^R \omega^r(x_m)}, \quad \sum_{r=1}^R v^r(x_m) = 1 \quad (6)$$

$$\tilde{y}_{im} = \sum_{r=1}^R v^r(x_m) \hat{y}_{im}^r(x_m) \quad (7)$$

where  $x_m = (x_{1m}, x_{2m})$  is  $m^{\text{th}}$  input vector resulted in  $\tilde{y}_m = (\tilde{y}_{1m}, \tilde{y}_{2m})$ . The consequent parameters are determined by solving optimization problem (8).

$$\|\tilde{e}\|^2 = \|\tilde{y} - \tilde{\tilde{y}}\|^2 \quad (8)$$

where  $\tilde{y} = (y_1^T, y_2^T, \dots, y_M^T)^T$  and  $\tilde{\tilde{y}} = (\tilde{y}_1^T, \tilde{y}_2^T, \dots, \tilde{y}_M^T)^T$ .

In cases where the antecedent part is designed using the FCM clustering procedure, the number of rules equals

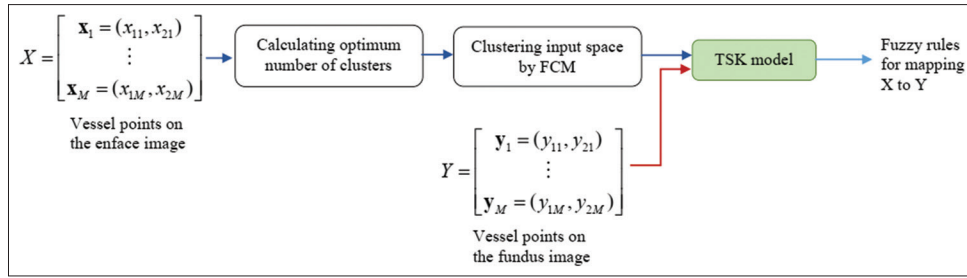


Figure 5: Block diagram of registration phase. FCM: Fuzzy C-Means, TSK: Takagi-Sugeno-Kang

the number of clusters and  $(F_1^r|_{x_{im}}, F_2^r|_{x_{2m}}) = u_{rm}$ , where  $F_i^r|_{x_{im}}$  is membership degree of  $x_{im}$ ,  $i = 1, 2$ . Given that,  $\vec{p} = (p_0^1 p_1^1 p_2^1 \dots p_0^R p_1^R p_2^R)^T$  is the consequent parameter vector, the matrix representation of equation (7) is:<sup>[25]</sup>

$$\vec{y} = H\vec{p} \quad (9)$$

$$H = \begin{bmatrix} u_{11} \cdot x_1 & \dots & u_{1c} \cdot x_1 \\ \vdots & \ddots & \vdots \\ u_{M1} \cdot x_M & \dots & u_{Mc} \cdot x_M \end{bmatrix} \quad (10)$$

Solving least-squares optimization (8) with Tikhonov regularization yields to optimum consequent parameter vector (11).

$$\vec{p} = \left( \frac{1}{const} I + H^T H \right)^{-1} H^T \quad (11)$$

## Experiment

### Data

#### Training dataset

The proposed algorithm requires a training phase for vessel extraction. Fundus vessel segmentation remains an open challenge, with several benchmark datasets available for evaluation. In our study, we used the DRIVE and CHASE\_DB1 fundus vessel benchmark datasets to train and validate the U-Net model. The total number of fundus images used was 68, which we split into 36 images for training and 32 images for validation. Since there is no existing benchmark dataset for en face vessel segmentation, we manually segmented 94 en face vessel images to create a ground truth dataset. From these, 75 images were used for training, and 19 were used for validation. It is important to note that for both en face and vessel segmentation, the data used to train the U-Net model are entirely different from the data used for the registration task; there is no overlap between the datasets.

#### Registration dataset

A dataset comprising retinal images from 44 normal cases and 29 cases with ocular abnormalities was used to evaluate the efficacy of the proposed algorithm. Each image pair includes a color fundus image and an OCT image

obtained using the Topcon 3D OCT-1000 instrument. The OCT images consist of varying numbers of slices, each with dimensions of  $650 \times 512$  pixels, while the fundus images have a resolution of  $1536 \times 2048$  pixels. The maximum number of slices is 128, although some subjects have missing slices. These data are publicly available at [https://misp.mui.ac.ir/fa/Comprehensive Topcon 3D-OCT Dataset: Inclusive of Normal and AbnormalOCT Volumes](https://misp.mui.ac.ir/fa/Comprehensive%20Topcon%203D-OCT%20Dataset%20Inclusive%20of%20Normal%20and%20AbnormalOCT%20Volumes).

### Implementation details

The U-Net model for retinal vessel segmentation is configured with several important hyperparameters that influence its performance. The learning rate, which is randomly selected between 0.0000005 and 0.0005, controls the step size during gradient descent, impacting the speed and stability of convergence. The model uses a batch size of 1, which processes one training sample per iteration, allowing for more precise updates but potentially slower training. It is trained over 500 epochs (chosen through trial and error), meaning the entire dataset is passed through the network 500 times, which helps the model learn the intricate patterns of retinal vessels. The ReLU activation function is applied throughout the network, introducing nonlinearity that enables the model to capture complex features. The Adam optimizer with momentum terms set to 0.5 and 0.999 is used, combining the benefits of adaptive learning rates and momentum to efficiently minimize the binary cross-entropy loss function.

## Results

Figure 6 illustrates the results of the proposed method for four sample cases. The extracted vessels from the fundus images are displayed in green, while the vessels from the en face images are shown in magenta. The yellow points represent the mapped points, which are the points on the en face vessels that have been registered onto the fundus vessels using fuzzy rules. It is important to note that not all en face vessel points are registered, as there may be no corresponding points on the fundus vessels. Corresponding points are determined based on their Euclidean distance.

To evaluate the effectiveness of the proposed method relative to alternative techniques, we implemented RANSAC with three commonly employed mathematical

**Table 1: Comparison of the proposed method with other methods on dataset 1**

Method	Absolute error ( $\mu\text{m}$ )			
	Mean $\pm$ SD		5 <sup>th</sup> , 50 <sup>th</sup> , and 95 <sup>th</sup> percentile	
	Superior–inferior	Nasal–temporal	Superior–inferior	Nasal–temporal
Proposed method	44.57 $\pm$ 39.38	11.46 $\pm$ 10.06	2.55, 33.48, 124.40	0.67, 8.65, 31.72
RANSAC with rigid model	73.14 $\pm$ 54.89	19.38 $\pm$ 14.36	2.13, 58.22, 181.99	0.67, 15.89, 47.06
RANSAC with affine model	94.43 $\pm$ 303.44	23.09 $\pm$ 41.59	2.90, 62.91, 188.64	0.86, 17.66, 51.56
RANSAC with similarity model	50.59 $\pm$ 49.28	13.75 $\pm$ 12.75	1.80, 38.62, 151.70	0.41, 10.71, 39.87
TPS-RPM	70.75 $\pm$ 52.66	18.64 $\pm$ 13.53	2.97, 55.84, 173.15	0.77, 15.02, 45.01

RANSAC – Random sample consensus; TPS-RPM – Thin-plate spline-robust point matching; SD – Standard deviation

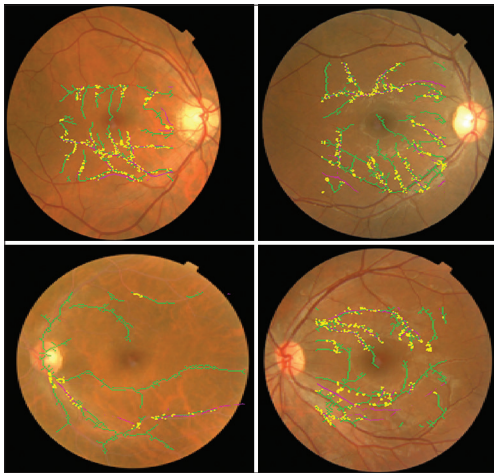


**Figure 6:** The extracted vessels from the fundus images are displayed in green, while the vessels from the en face images are shown in magenta. The yellow points represent the mapped points, which are the points on the en face vessels that have been registered onto the fundus vessels using fuzzy rules

models: rigid, affine, and transformations. In addition, we included the well-established thin-plate spline-robust point matching algorithm,<sup>[26]</sup> which is renowned for its point matching capabilities, for comparison. A quantitative evaluation, detailed in Table 1, highlights the superiority of the proposed method over the other algorithms.

The proposed algorithm takes approximately 0.2 s to execute, which is about 10 times slower than other methods. However, time efficiency is not a primary concern, as real-time performance is not essential for this application. That said, a 0.2-s processing time is still sufficient for real-time use if needed.

## Conclusion

This article introduces a nonrigid image registration method based on fuzzy theory for the registration of multimodal retinal images. Given the distinct properties of information in each modality, we focus on utilizing common features, specifically the positions of retinal vessels, across modalities. Our proposed algorithm effectively registers fundus images and en face images obtained from OCT B-scans. Experimental results demonstrate that our method outperforms state-of-the-art techniques, highlighting its potential to enhance the accuracy of multimodal retinal image

alignment. This advancement holds promise for improving diagnostic accuracy and treatment planning in ophthalmology.

## Acknowledgment

This work was supported by the Iran National Science Foundation.

## Financial support and sponsorship

Nil.

## Conflicts of interest

There are no conflicts of interest.

## References

- Bernardes R, Serranho P, Lobo C. Digital ocular fundus imaging: A review. *Ophthalmologica* 2011;226:161-81.
- Schmitt JM. Optical coherence tomography (OCT): A review. *IEEE J Sel Top Quantum Electron* 1999;5:1205-15.
- Jiao S, Knighton R, Huang X, Gregori G, Puliafito C. Simultaneous acquisition of sectional and fundus ophthalmic images with spectral-domain optical coherence tomography. *Opt Express* 2005;13:444-52.
- Stopa M, Bower BA, Davies E, Izatt JA, Toth CA. Correlation of pathologic features in spectral domain optical coherence tomography with conventional retinal studies. *Retina* 2008;28:298-308.
- Amini Z, Kafieh R, Tajmirrahi M, Parsons Z, Rabbani H. Application of enface image registration/alignment to introduce new ocular imaging biomarkers. In: *Photo Acoustic and Optical Coherence Tomography Imaging*. Vol. 2. Bristol, UK: IOP Publishing; 2022. p. 3-1-3-23.
- Mokhtari M, Rabbani H, Mehri-Dehnavi A. Alignment of Optic Nerve Head Optical Coherence Tomography B-Scans in Right and Left Eyes. In *2017 IEEE International Conference on Image Processing (ICIP)*. IEEE; 2017. p. 2279-83.
- Mahmudi T, Kafieh R, Rabbani H, Mehri A, Akhlaghi MR. Evaluation of asymmetry in right and left eyes of normal individuals using extracted features from optical coherence tomography and fundus images. *J Med Signals Sens* 2021;11:12-23.
- Golabbakhsh M, Rabbani H. Vessel-based registration of fundus and optical coherence tomography projection images of retina using a quadratic registration model. *IET Image Process* 2013;7:768-76.
- Lee J, Liu P, Cheng J, Fu H. A deep step pattern representation for multimodal retinal image registration. *Proc IEEE Int Conf Comput Vis* 2019;2019:5076-85.
- Li Y, Gregori G, Knighton RW, Lujan BJ, Rosenfeld PJ.

- Registration of OCT fundus images with color fundus photographs based on blood vessel ridges. *Opt Express* 2011;19:7-16.
11. Mokhtari M, Rabbani H, Mehri-Dehnavi A, Kafieh R, Akhlaghi M, Pourazizi M, *et al.* Local comparison of cup to disc ratio in right and left eyes based on fusion of color fundus images and OCT B-scans. *Inf Fusion* 2019;51;30-41.
  12. Rivas-Villar D, Hervella ÁS, Rouco J, Novo J. Joint keypoint detection and description network for color fundus image registration. *Quant Imaging Med Surg* 2023;13:4540-62.
  13. Sindel A, Hohberger B, Maier A, Christlein V. Multi-modal retinal image registration using a keypoint-based vessel structure aligning network. In: *Lecture Notes in Computer Science (Including Subseries Lecture Notes in Artificial Intelligence and Lecture Notes in Bioinformatics)*. Vol. 13436. Cham, Switzerland: LNCS; 2022. p. 108-18.
  14. Kalantari R, Moqadam R, Loghmani N, Allahverdy A, Shiran MB, Zare-Sadeghi A. Brain tumor segmentation using hierarchical combination of fuzzy logic and cellular automata. *J Med Signals Sens* 2022;12:263-8.
  15. Narayan V, Mall PK, Awasthi S, Srivastava S, Gupta A. FuzzyNet: Medical Image Classification Based on GLCM Texture Feature. In: *2023 International Conference on Artificial Intelligence and Smart Communication (AISC)*. IEEE; 2023. p. 769-73.
  16. Hurtík P, Perfilieva I, Hodáková P. Fuzzy transform theory in the view of image registration application. In: *Communications in Computer and Information Science*. Part. 2. Vol. 443. Cham, Switzerland: CCIS; 2014. p. 143-52.
  17. Hosseini MS, Moradi MH, Tabassian M, D'hooge J. Non-rigid image registration using a modified fuzzy feature-based inference system for 3D cardiac motion estimation. *Comput Methods Programs Biomed* 2021;205:106085.
  18. Weng W, Zhu X. UNet: Convolutional networks for biomedical image segmentation. *IEEE Access* 2021;9:16591-603.
  19. Alom MZ, Hasan M, Yakopcic C, Taha TM, Asari VK. Recurrent residual convolutional neural network based on U-Net (R2U-Net) for medical image segmentation. *arXiv preprint arXiv:1802.06955*; 2018. [doi: 10.48550/arXiv.1802.06955].
  20. Daszykowski M, Walczak B. "2.29 - Density-Based Clustering Methods." In: Brown SD, Tauler R, Walczak B, editors. *Comprehensive Chemometrics: Chemical and Biochemical Data Analysis*. Vol. 2. Oxford, UK: Elsevier; 2009. pp. 635-54. doi: 10.1016/B978-044452701-1.00067-3.
  21. Bezdek JC, Ehrlich R, Full W. FCM: The fuzzy c-means clustering algorithm. *Comput Geosci* 1984;10:191-203.
  22. Takagi T, Sugeno M. Fuzzy identification of systems and its applications to modeling and control. *IEEE Trans Syst Man Cybern* 1985;SMC-15:116-32.
  23. Sugeno M, Kang G. Structure identification of fuzzy model. *Fuzzy Sets Syst* 1988;28:15-33.
  24. Männle M. Identifying Rule-Based TSK Fuzzy Models. *Proc Eur Congr Intell Tech Soft Comput. (EUFIT 1999)*, Aachen, Ger Elit Found; 1999. p. 286-99. Available from: [http://www.maennle.org/manfred/publications/19990901\\_eufit99.pdf](http://www.maennle.org/manfred/publications/19990901_eufit99.pdf). [Last accessed on 2025 Jan 15].
  25. Davoodi R, Moradi MH. Mortality prediction in intensive care units (ICUs) using a deep rule-based fuzzy classifier. *J Biomed Inform* 2018;79:48-59.
  26. Chui H, Rangarajan A. A new point matching algorithm for non-rigid registration. *Comput Vis Image Underst* 2003;89:114-41.